

Article

TiO₂–Graphene Oxide and TiO₂–Reduced Graphene Oxide Composite Thin Films for Solar Photocatalytic Wastewater Treatment

Ioana Tismanar ¹, Alexandru Cosmin Obreja ², Octavian Buiu ² and Anca Duta ^{1,3,*}¹ R&D Center Renewable Energy System and Recycling, Transilvania University of Brasov, 500036 Brasov, Romania² National Institute for Research and Development in Microtechnologies, IMT-Bucharest, 077190 Ilfov, Romania³ Technical Sciences Academy of Romania, 030167 Bucharest, Romania

* Correspondence: a.duta@unitbv.ro

Abstract: This research reports on Vis- and solar-active photocatalytic bi-layered films of TiO₂ (layer 1) and a composite with TiO₂ matrix and graphene oxide or reduced graphene oxide filler (layer 2) obtained by coupling two methods: spray pyrolysis deposition followed by spraying a diluted sol. The thin films crystallinity degree, surface morphology and elemental composition were recorded and the composites were tested in photo-degradation processes, using the standard 10 ppm methylene blue solution, under simulated UV + VIS irradiation conditions using an irradiance measured to be close to the natural one, in continuous flow process, at demonstrator scale; these results were compared with those recorded when using low irradiance values in static regime. The effect of the increase in the graphene oxide content was investigated in the concentration range 1.4%_w...10%_w and was found to increase the process efficiency. However, the photocatalytic efficiencies increased only by 15% at high irradiance values compared with the values recorded at low irradiance as result of the electron-hole recombination in the composite-thin film. Similar experiments were run using composites having reduced graphene oxide as filler. The interfaces developed between the matrix and the filler were discussed outlining the influence of the filler's polarity. The thin films stability in aqueous medium was good, confirmed by the results that outlined no significant differences in the surface aspect after three successive photocatalytic cycles.

Keywords: TiO₂-(r)GO composite photocatalyst; TiO₂-(r)GO stability; thin film photocatalysts; VIS-active photocatalyst; continuous flow photocatalytic processes

Citation: Tismanar, I.; Obreja, A.C.; Buiu, O.; Duta, A. TiO₂–Graphene Oxide and TiO₂–Reduced Graphene Oxide Composite Thin Films for Solar Photocatalytic Wastewater Treatment. *Energies* **2022**, *15*, 9416. <https://doi.org/10.3390/en15249416>

Academic Editor: Junlian Wang

Received: 18 November 2022

Accepted: 8 December 2022

Published: 12 December 2022

Publisher's Note: MDPI stays neutral with regard to jurisdictional claims in published maps and institutional affiliations.



Copyright: © 2022 by the authors. Licensee MDPI, Basel, Switzerland. This article is an open access article distributed under the terms and conditions of the Creative Commons Attribution (CC BY) license (<https://creativecommons.org/licenses/by/4.0/>).

1. Introduction

The world population growth along with the climate change issues related to the required water amounts mainly for residential and industrial applications were outlined as a challenge in Europe and not only. The European Commission estimates that a significant part of the EU countries already faces problems related to the water supply and by 2025, at world level, over 3.5 billion people will face the “water stress”, (UE Directive, 2000/60/EC) [1]. In this context, the wastewater treatment plants represent a viable alternative to deliver water for reuse in various applications. However, as the parameters formulated for water reuse are commonly not fulfilled by the conventional wastewater treatment processes, new advanced technologies and materials are required to overcome this limit that is mainly related to the low but still above the reuse concentration level of pollutants in the treated wastewater.

The photocatalytic processes are intensively investigated for the advanced wastewater treatment to remove organic emergent pollutants at low concentrations, e.g.,

phenolic compounds, pharmaceuticals, pesticides or dyes. Nonselective oxidation species are involved in the pollutants removal reactions, mainly the hydroxyl radical ($\text{HO}\cdot$) but also the superoxide radical anion (O_2^-). These species are the result of the oxidation and reduction reactions of the charge carriers (electrons and holes) produced at the surface of a semiconductor photocatalytic material when irradiated with suitable radiation [2]. Most of the aqueously stable and efficient photocatalysts are wide band gap semiconductors activated by UV radiation, leading to high process costs. It is therefore required to expand their photocatalytic response towards VIS (or towards most of the solar spectral range), to reduce these costs and support up-scaling.

Titanium dioxide (TiO_2) is a wide band gap semiconductor ($E_g = 3.0\text{--}3.2\text{ eV}$) activated by UV irradiation [3]. Despite the activation energy, TiO_2 is the most widely reported photocatalyst because of its stability in a wide range of pH that makes it suitable for the advanced wastewater treatment aimed at reuse. Moreover, titanium dioxide is non-toxic and has an acceptable production cost.

For the advanced wastewater treatment, many research groups are working to overcome the limitation imposed by the UV activation that involves huge costs associated with material activation, thus leading to economically disadvantageous processes. Recent papers focus on novel composite materials with TiO_2 matrices to be activated under Vis or solar irradiation. A highly investigated VIS-activation route consists of developing heterostructures by coupling a wide band gap n-type semiconductor with a narrow band gap p-type semiconductor [4] with suitably aligned energy bands [5]. Literature mainly mentions heterostructures with *n-p* hetero-junctions of the diode type or following a Z-scheme [6]. The difference between these is mainly related to the photocatalyst activation (using UV or Vis or solar radiation), depending on the semiconductors in the hetero-structure.

Recently, p-type semiconductors such as the graphene derivatives (graphene oxide, GO, or reduced graphene oxide, rGO) were outlined as a viable option for coupling with TiO_2 mainly because of their remarkable aqueous stability [7]. The association of TiO_2 with graphene derivative fillers leads to the formation of Vis-active composites, materials that can be easily activated by the cost-free solar radiation. These composites allow the formation of hetero-structures following the suitable energy bands alignment as presented in Figure 1.

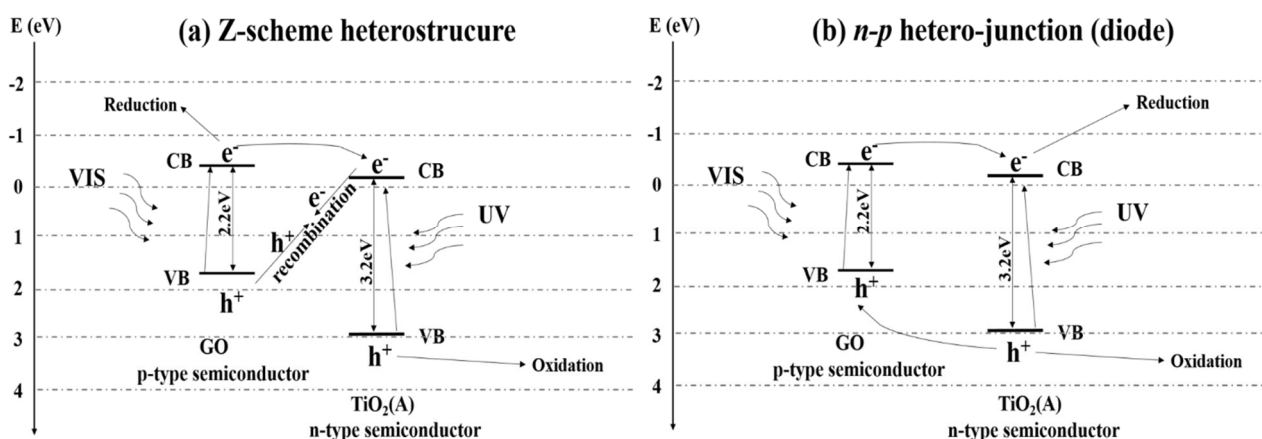


Figure 1. Energy bands alignment in the TiO_2 (A) anatase–GO hetero-structure: (a) Z-scheme hetero-structure and (b) *n-p* hetero-junction (diode).

In a Z-scheme hetero-structure consisting of TiO_2 and GO, as presented in Figure 1a, the activation may mainly occur under UV radiation as the holes, the main charge carrier responsible for the pollutant's degradation, can only be produced under UV irradiation. Moreover, only half of the generated charge carriers will be involved in the photocatalytic mechanism, the other half being the subject of recombination [8]. To produce an efficient

solar- or Vis-active Z-scheme hetero-structure, an electron mediator should be thus inserted in the system [9,10].

If the hetero-structure proves to be efficient under solar- or Vis radiation, the most likely mechanism will correspond to an *n-p* diode type hetero-junction, Figure 1b. This type of structure well supports the efficient charge carrier's transfer at the semiconductors level, limiting the electron-hole recombination, thus increasing the process efficiency under Vis (thus, also solar) activation [11,12].

The chemical Ti-O-C bonds developed among TiO₂ and the graphene derivative functional groups (hydroxyl, epoxy, carbonyl, carboxyl) lead to the development of continuous interfaces that confirm the components compatibility in the composite [13]. The differences between the GO and the rGO fillers are mainly related to their polarity, which is the direct consequence of the percentage of groups containing oxygen in the 2D carbon structure. The GO polarity is the result of the functional groups and of the network defects that support the random diffusion of the charge carriers. While graphene has a semi-metallic behavior, graphene oxide is considered a semiconductor or even an insulator depending on the oxidation degree, following the sp² to sp³ change in hybridization of the carbon atoms leading to a permanent band gap [14]. The lower percentage of the oxygen-containing functional groups in rGO as compared to GO will increase its semi-metallic behavior, similar to that of graphene. However, graphene oxide with reduced functional groups (rGO) has network defects and is considered a semiconductor with a variable band gap energy depending on the residual oxygen containing groups that are still in the structure after reduction [15]. The GO and the rGO fillers support the photocatalytic process by developing composites with strong, Vis-active interfaces; these composites also have good wetting properties and a large specific surface area available for the pollutant(s) adsorption.

For the up-scaled use of these materials, the production and the process costs have also to be considered. Photocatalytic powders were mostly investigated because of their higher photocatalytic efficiencies but the additional cost related to the advanced filtration needed after the process make their use unprofitable. The use of thin films represents a viable option to avoid this additional cost and preserve the photocatalytic material for reuse, thus avoiding losses. These films have a lower specific surface area compared to the powders, therefore the photocatalytic films should have high average surface roughness and optimum surface charge able to support the adsorption of a significant amount of pollutant molecules as a pre-requisite for a good photo-degradation efficiency.

Only few studies report on up-scaled photocatalytic processes at the demonstrator level using powder photocatalysts [16,17]. Thin films were, to the best of our knowledge, not so far reported for up-scaled implementation. The process parameters that have to be considered and optimized are in this case similar with those considered when using powders, as:

- (1) The spectral range and the irradiance value required to activate the photocatalyst to produce the electron-hole pairs (it is expected that the higher the radiation intensity, the higher the amount of produced charge carriers);
- (2) The photocatalyst specific and overall surface correlated with the volume of the pollutant solution that is subject of treatment;
- (3) The pH of the wastewater, correlated with the point of zero charge (PZC) of the photocatalyst, selected to support the pollutant-photocatalyst attraction, thus increasing the overall efficiency of the processes;
- (4) The hydrophilicity of the photocatalytic surface that is important in the pollutant removal in the advanced wastewater treatment.

This paper reports on bi-layered composite thin films with the structure TiO₂/TiO₂-GO or TiO₂/TiO₂-rGO, obtained by coupling two low-cost and up-scalable techniques: spray pyrolysis deposition (SPD) and sol-gel synthesis followed by spraying. These pho-

photocatalytic structures were selected to support the ordered growth of the second composite thin layer over the first crystalline layer without the need of a very high temperature treatment of the composite structure, as required by the filler (GO or rGO) thermal stability, up to 170...180 °C [18]. These types of two-layered composite thin films were previously developed in our research group as novel photocatalysts [19], to investigate the possibility to use them as Vis-active photocatalysts. Moreover, this paper reports on composite photocatalysts developed to be used as stable films in an optimized continuous flow demonstrator installation, in photocatalytic processes using as wastewater the standard methylene blue (MB) dye solution [20], under simulated solar (UV + Vis) irradiation using irradiance close to the natural ones ($G_{\text{total}} = 810 \text{ W/m}^2$). Thus, the paper proposes competitive novel photocatalytic thin film composites deposited on large substrate surfaces to be used in up-scaled applications in process conditions similar to those found in small wastewater treatment plants, considering and optimizing the process parameters. The results were compared with those recorded at low irradiance values ($G_{\text{total}} = 55 \text{ W/m}^2$) at laboratory scale, in static regime using optimized process conditions (optimized pH of the pollutant solution). The filler type and content influence was analyzed along with the film's stability at the high irradiance values used during testing.

2. Materials and Methods

For deposition glass plate substrates covered with FTO (F-doped SnO_2)-(Pilkington TEC15) were used. Before use, each substrate was cleaned under sonication (Dekang, DK-600H ultrasound bath) using a mix of deionized water and detergent. Further on, the substrates were rinsed in ethanol and were then dried in air. For the photocatalytic tests, a $20 \times 30 \text{ cm}^2$ photocatalytic thin film surface was inserted in the photocatalytic demonstrator reactor, Figure 2 [21]. The overall surface contains five $10 \times 10 \text{ cm}^2$ plates, one plate of $8 \times 10 \text{ cm}^2$ and five $2 \times 2 \text{ cm}^2$ small plates that were used for characterization before and after the process to assess the films stability. For the experiments run at laboratory scale, in static regime, $1.5 \times 1.5 \text{ cm}^2$ FTO glass plates were used as substrates.

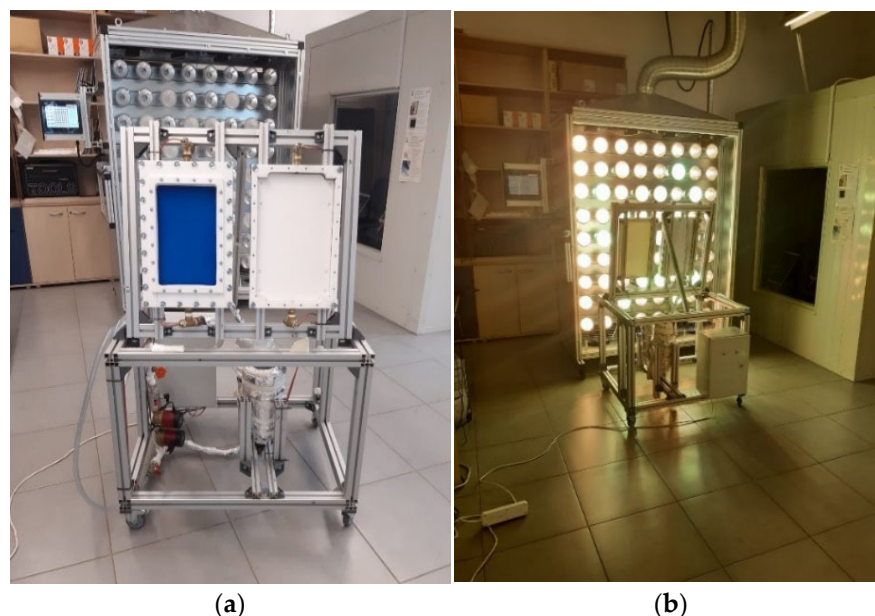


Figure 2. The photocatalytic demonstrator reactor used in the experiments run in continuous flow (dynamic regime) (a) front view and (b) back view of the demonstrator

The photocatalytic composites were deposited on the FTO substrates following two steps:

- (1) A first layer consisting only of TiO_2 was deposited by SPD using an ABB/IRB2400L robot (air carrier gas and 1.2 bar pressure). The precursor system was a solution of titanium tetra-isopropoxide as precursor (TTIP), acetylacetone complexing agent (AcAc) and ethanol solvent (EtOH) mixed in a volume ratio of 1:1:15, as previously described [19]. This precursor system was sprayed at 400 °C using eight sequences and a break of 60 s between two deposition sequences. After deposition, an annealing treatment for 3 h at 450 °C was applied to this first layer in an oven (Nabertherm, LE14/11/B150), to reach an admissible crystallinity degree.
- (2.a) A second layer was deposited using a sol of the composite with TiO_2 matrix and GO filler (TiO_2 -GO composite) sprayed on the top of the TiO_2 first layer. The sol system consisted of a mix of TTIP, EtOH, AcAc and acetic acid in a 1:0.8:0.04:0.009_(v) ratio, as previously described [19]. An aqueous GO dispersion ($c = 30 \text{ mg/mL}$) was prepared by the originally modified Hummers and Offeman method [22,23]. This GO dispersion was added slowly and under continuous stirring to the sol system, to get the composite dispersion. Four GO contents were investigated, with the weight ratios of 1.4%_w, 3%_w, 5%_w and 10%_w in the precursor system.
- (2.b) Another second layer consisting of the TiO_2 -rGO composite was also deposited by spraying a sol on the TiO_2 first layer. The rGO ethanolic dispersion (26.3 mg/mL) was obtained by reducing the GO aqueous dispersion. Firstly, N-Methyl-2-pyrrolidone (NMP) was added and then the GO dispersion was reduced to rGO using a hydrazine hydrate 25% solution at 80 °C under continuous stirring for 1 h. The mixture was then repeatedly centrifuged six times to remove the water and the NMP and replace these with absolute ethanol. The ethanolic dispersion was placed for one hour in an ultrasound bath to support the rGO sheets exfoliation [21]. The composite sol was prepared using titanium tetra-isopropoxide (TTIP), the rGO ethanolic dispersion, ethanol (EtOH), acetylacetone (AcAc), acetic acid (HAc) and deionized water in a TTIP:rGO:EtOH:AcAc:HAc:H₂O = 1: 0.52: 0.28: 0.04: 0.009: 0.12_(v) volume ratio. Following this ratio, the rGO content in the precursor system was calculated to be 5%_w.

After synthesis, the composite sols of TiO_2 with the GO or with the rGO filler were sonicated (using the ultrasound bath, Dekang, DK-600H) for 1.5 h and further diluted using ethanol in a volume ratio sol: EtOH = 1:5, as previously optimized [19]. The same ABB/IRB2400L robot (air carrier gas and 1.2 bar pressure) was used to deposit the diluted sol using twelve spraying pulses with 60 s break between two pulses. The sols were sprayed at 100 °C to support the elimination of the continuous medium (EtOH), followed by the thermal treatment for one hour at 150 °C to remove the potential by-products from the sol dispersion in the thin films, but avoiding the oxidation of the GO or rGO fillers [18].

Five composite structures were deposited as thin films: FTO/ TiO_2 / TiO_2 -GO 1.4%_w; FTO/ TiO_2 / TiO_2 -GO 3%_w; FTO/ TiO_2 / TiO_2 -GO 5%_w; FTO/ TiO_2 / TiO_2 -GO 10%_w and FTO/ TiO_2 / TiO_2 -rGO 5%_w. A reference layer was also deposited with the same double-layered structure but without filler in the second layer (FTO/ TiO_2 / TiO_2 no filler). Moreover, a sample with the first SPD layer (code FTO/ TiO_2) was also investigated.

The characterization of the samples was done using X-ray diffraction (XRD, Bruker D8 Discover, step size 0.024, scan speed 1.5 s/step, 2 θ range from 5 to 70°) and the Diffrac. EVA 5.0 software to evaluate the crystallinity degree. The surface elemental composition was investigated using Energy Dispersive X-ray spectrometry (EDX, Thermo).

The surface morphology and the thickness of the deposited samples were analyzed using scanning electron microscopy (SEM, Hitachi model S-3400 N type II) and the average surface roughness (RMS) was estimated using atomic force microscopy (AFM, NT-MDT model BL222RNTE).

The PZC of the films was estimated by potentiometric titration (SI Analytic Titroline 6000 Titrator). Each thin film was immersed in a NaOH 0.1 N solution and titrated with HCl 0.1 N solution.

The wettability of the composites was estimated by water contact angle (WCA) measurements using a DataPhysics GmbH OCA 20 Instruments device with the volume of the water droplet of 10 μ L.

The photodegradation experiments were run in static and in dynamic regime to estimate the photocatalytic efficiency of the 1.5×1.5 cm² and of the 20×30 cm² films using a 10 ppm ($3.125 \cdot 10^{-5}$ M) methylene blue (MB, Scharlau, C.I.52015) aqueous solution, as recommended by the standard [20]. During the photocatalytic experiments, the pollutant solution pH was selected targeting the increase in the pollutant adsorption, considering the PZC value of the photocatalyst. In the continuous flow (dynamic) regime, the photodegradation tests used 5L of MB pollutant solution. The flow of the pollutant in the demonstrator reactor was 1L/min and the thickness of the aqueous layer over the photocatalyst was of 20 mm, as previously reported [21]. In the beginning, the process ran for one hour in the dark and, as earlier observed, one hour represents a contact time long enough to reach the adsorption/desorption equilibrium [19]. Then, the photocatalytic reactor with a quartz upper plate was continuously irradiated for 5 h using a homemade solar simulator (Figure 2) and the pollutant residual concentration was evaluated hourly. The average irradiance value, measured using a Delta-T, type BF3 pyranometer on the photo-reactor's upper plate, was $G = 810$ W/m², out of which 23 W/m² corresponded to the UV radiation and the rest to VIS. The photodegradation tests were run in three successive cycles using in each cycle freshly prepared MB 10 ppm solution to estimate the films stability. Before the first photocatalytic cycle, each thin photocatalytic film was conditioned by one hour exposure to UV radiation ($G = 23$ W/m²) to support the photocatalytic surface to reach super-hydrophilicity. After each photocatalytic cycle, the plates with the photocatalytic films were cleaned in the demonstrator using a deionized water flow, for 30 min, to remove possible traces of the remaining pollutant or of the degradation by-products. Afterwards, before the second and the third cycle, the plates were firstly wetted with deionized water and were irradiated for 2 h using UV + VIS radiation ($G_{\text{total}} = 810$ W/m² with 23 W/m² corresponding to UV) to regenerate/self-clean the surface along with the film conditioning. The absorbance spectra of the films after photocatalysis and after regeneration were recorded using a UV–VIS–NIR spectrophotometer (Perkin Elmer Lambda 950) to estimate the self-cleaning efficiency [24].

The kinetics of the dye photo-degradation process was investigated during the first testing cycle run in dynamic regime. The process data were linearized according to the pseudo-first order kinetic [25,26], following Equation (1):

$$\ln C_t = \ln C_0 - kt \quad (1)$$

where: C_0 : the initial MB concentration, C_t : the concentration of MB at moment t , k : the reaction rate constant.

Parallel experiments were run in static regime (without any flow of the pollutant solution) using a laboratory scale reactor equipped with “2 UV (Philips, TL-D BLB 18W/108) and 5 VIS light tubes (Philips, TL-D Super 80 18W/865)”. The average total irradiance value was $G_{\text{total}} = 55$ W/m², with 3 W/m² corresponding to the UV. This UV + VIS configuration simulates the radiation delivered by the solar simulator but at a much lower irradiance value (and a slightly higher UV share) and allows investigating the effect of the photons flux on the process. The film was immersed in 20 mL of MB solution in a quartz beaker of 50 mL and was kept for one hour without irradiation (in the dark) followed by 5 h of irradiation.

The photocatalytic efficiency of each type of (multi)layered material, η_t , was calculated using Equation (2), where A_0 represents the initial MB solution absorbance and A_t

represents the absorbance after t hours of the process, measured at the absorbance wavelength of the pollutant ($\lambda_{\text{MB max}} = 665 \text{ nm}$), using an UV–VIS–NIR spectrophotometer (Perkin Elmer Lambda 950):

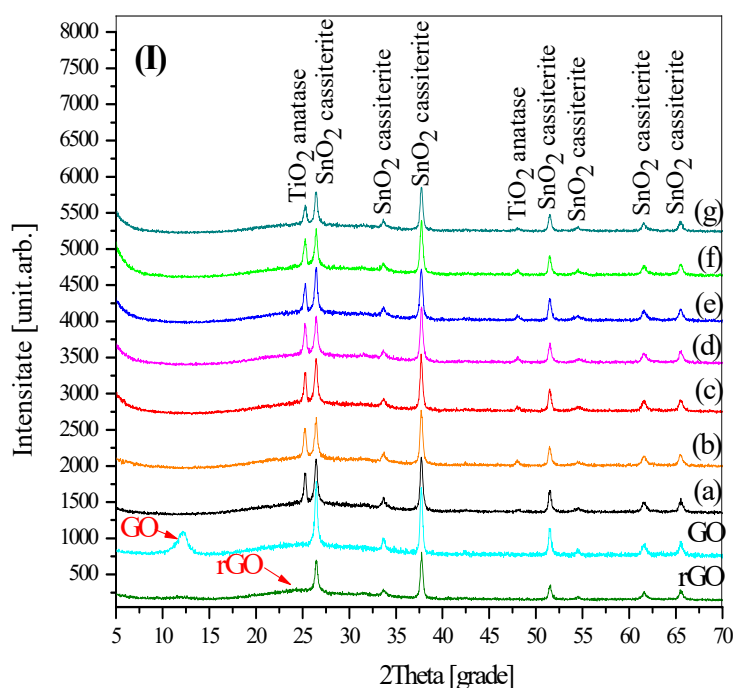
$$\eta_t = \frac{A_0 - A_t}{A_0} \cdot 100 \quad (2)$$

The stability of the films was estimated after each photocatalytic cycle based on the changes in the morphology, composition and average roughness variation of the composite thin films. The change of the crystallinity degree after the third photocatalytic cycle was analyzed to further estimate the photocatalyst stability.

3. Results and Discussions

In Figure 3I are presented the XRD results for the fillers (GO and rGO) deposited on the FTO substrate and for the mono- and bi-layered thin films before use. The pattern of GO shows the characteristic peak at $2\theta = 12.1^\circ$ [27]. The reduction of GO to rGO provide the shift of the GO peak from 12.1° to the characteristic rGO large peak at $2\theta = 24.1^\circ$ [28]. However, the rGO peak is not clearly distinct following the lack of highly ordered rGO structures in the material.

All the thin films in the a–g graphs in Figure 3I outline the peaks associated with the anatase TiO_2 polymorph at $2\theta = 25.2^\circ$ and $2\theta = 48.0^\circ$ but also the characteristic peaks corresponding to the SnO_2 cassiterite polymorph from FTO. These substrate peaks confirm the deposition of the mono- and double-layers as very thin films. The absence of the peak(s) corresponding to the fillers in the composite films, in Figure 3Ic–g, may be the result of the chemical bonds partially developed between TiO_2 and (r)GO.



Thin Film	Crystallinity Degree [%]
(a) FTO/ TiO_2	37.7
(b) FTO/ TiO_2 / TiO_2 -no filler	40.3
(c) FTO/ TiO_2 / TiO_2 -GO 1.4% _w	42.5
(d) FTO/ TiO_2 / TiO_2 -GO 3% _w	44.5
(e) FTO/ TiO_2 / TiO_2 -GO 5% _w	45.2
(f) FTO/ TiO_2 / TiO_2 -GO 10% _w	45.1
(g) FTO/ TiO_2 / TiO_2 -rGO 5% _w	43.5

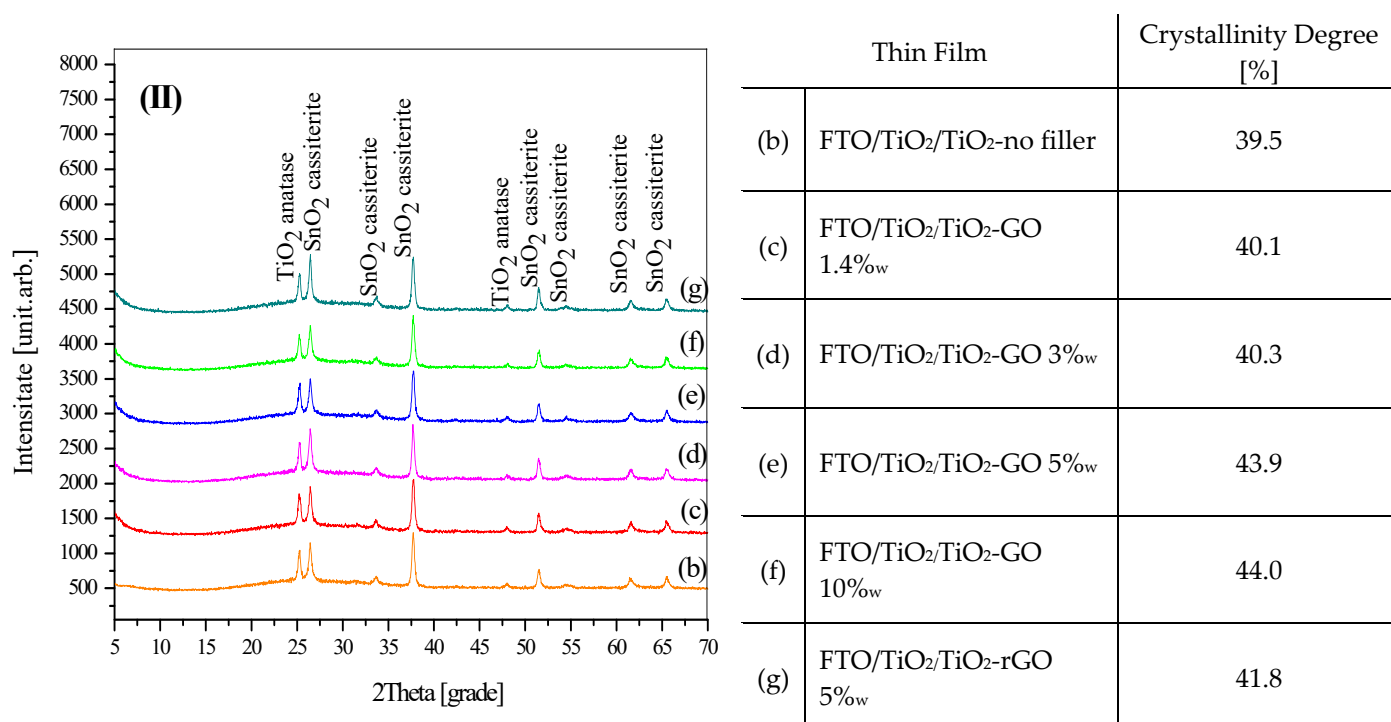


Figure 3. XRD patterns and crystallinity degree of the thin films: (I) before photocatalysis and (II) after the third photocatalytic cycle.

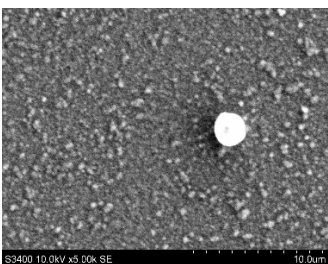
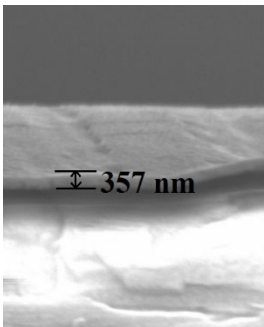
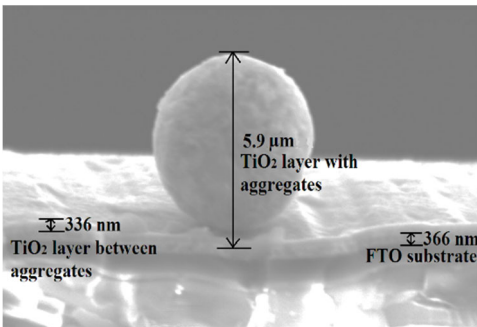
The (slightly) higher crystallinity degree of the two-layered reference film, without (r)GO filler in Figure 3 (I) graph (b), compared with the first layer confirms that the double layered structure leads to an increase in the overall crystallinity degree even if a low thermal treatment temperature was used (150 °C) for the thin second layer deposition. The increase in the crystallinity degree confirms the ordered growth of the composite thin film over the first crystalline layer.

The highest crystallinity degree corresponds to the composites with 5%_w and 10%_w GO, with an almost identical value; considering this result, these films are potentially the most efficient in photocatalysis as an ordered structure well supports the reduced recombination of the photogenerated charge carriers. The crystallinity degree of the FTO/TiO₂/TiO₂-rGO 5%_w composite also confirms the assumption of ordered growth over the first TiO₂ film. The slight differences in the crystallinity degrees between the composites with GO vs. rGO filler may be the result of the stronger interfaces developed not only in the second thin film layer but also with the first layer when using the GO filler.

The thin films stability was estimated after each cycle in dynamic regime based on the SEM images, the EDX results and the roughness values. The XRD results were recorded after the third photocatalytic cycle to evaluate the stability of the crystalline structure (Figure 3II). The results outline almost similar patterns and values before and after the third cycle; however, a slight crystallinity decrease especially for the thin films with 1.4%_w and 3%_w GO may be noticed suggesting that the photocatalyst with a low filler content may have a less good stability in the working condition.

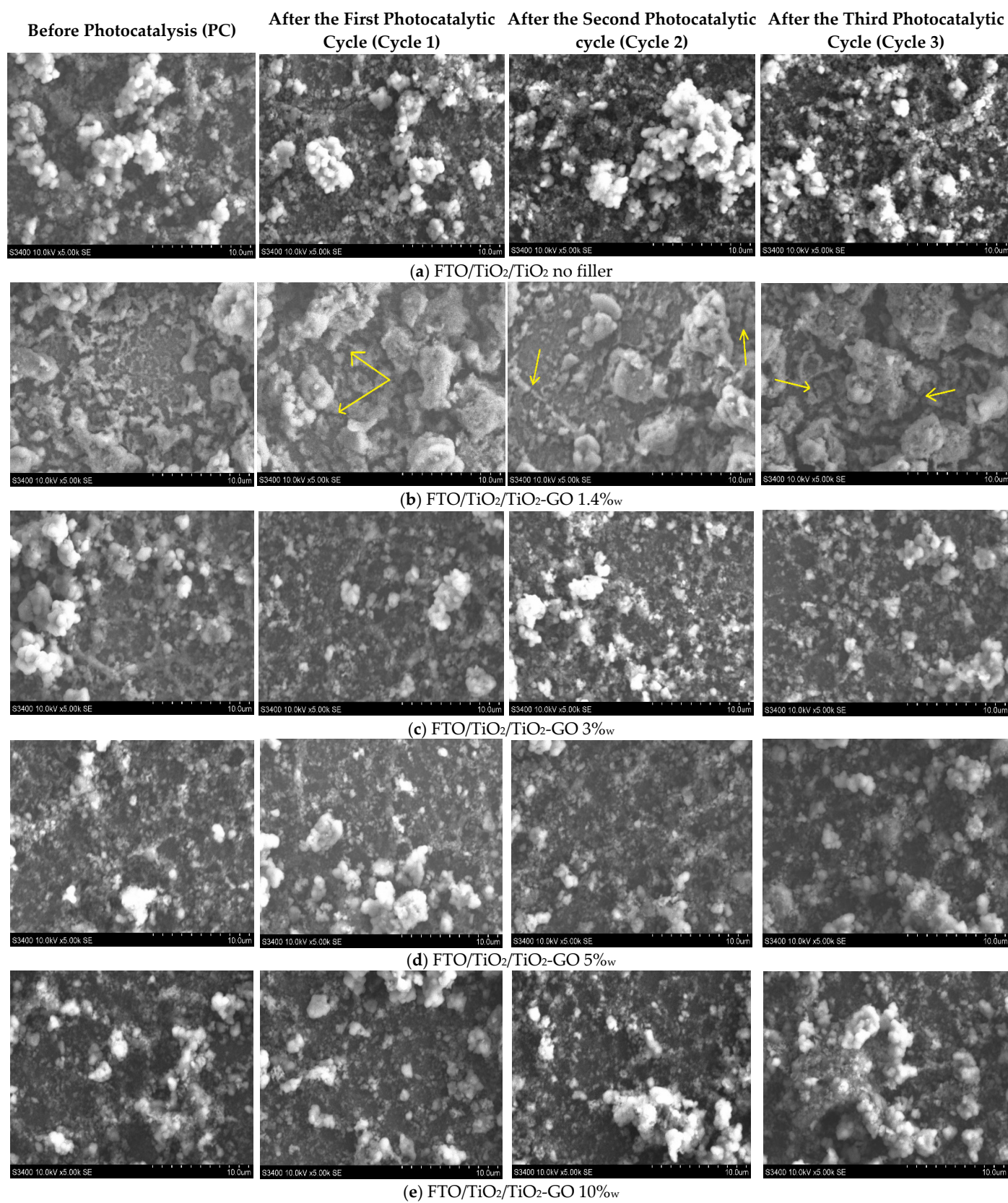
Morphology, surface composition and average surface roughness characterization was developed for the first TiO₂ layer and the results are included in Table 1.

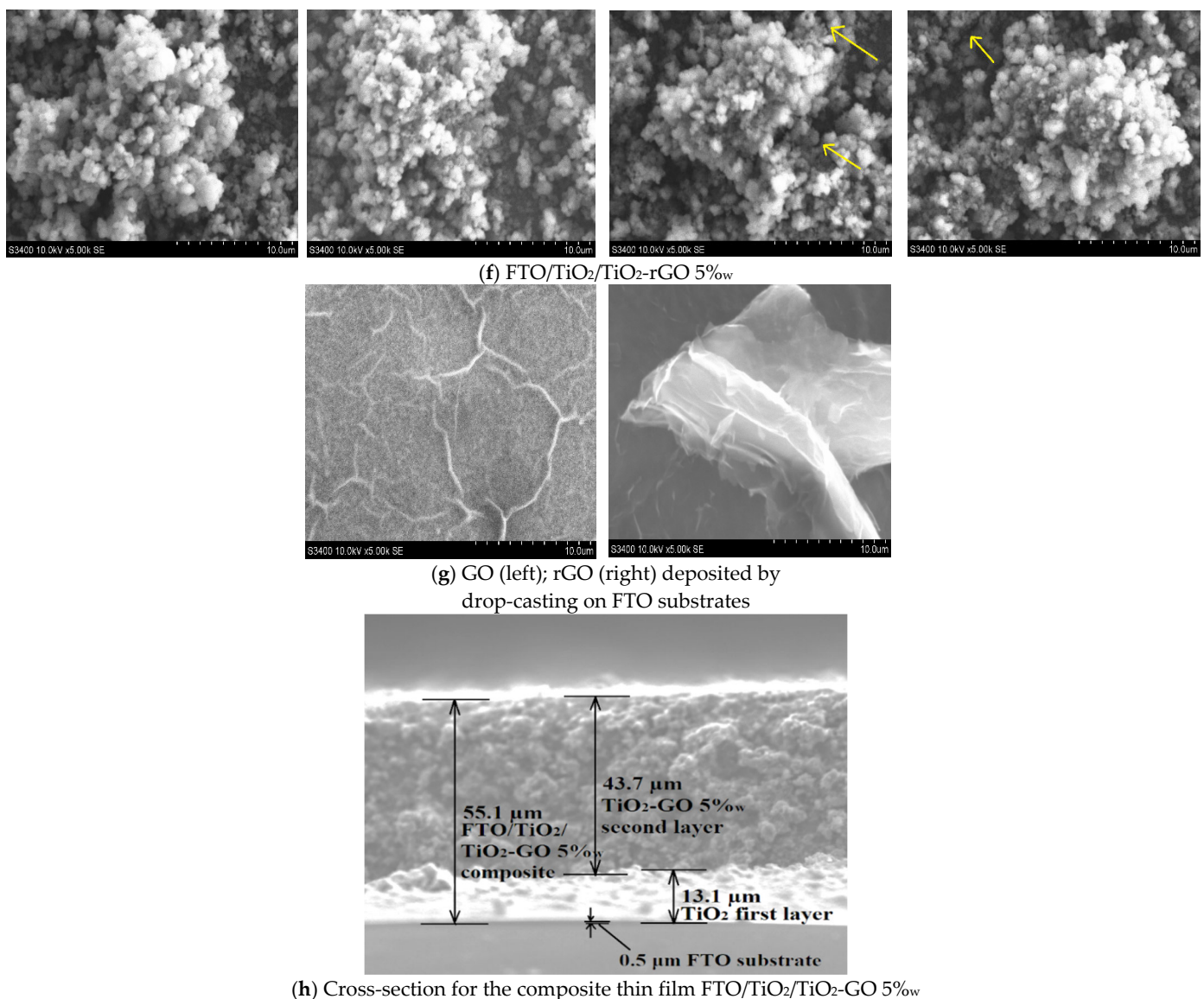
Table 1. Characterization results for the first TiO₂ layer: SEM images, surface elemental composition and average roughness.

Thin Film	SEM Images	Elemental Average Composition [at%]	RMS [nm]
FTO/ TiO ₂	 <p>Surface morphology</p>   <p>Cross-sections for the FTO substrate (left) and for the first TiO₂ layer on the FTO substrate (right)</p>	C: 0.00 Ti: 24.43 O: 66.66 F: 0.00 Sn: 8.71 Si: 0.21	15.0

The morphology analysis of the first layer outlines a rather uniform deposition. The surface aggregates may act as growth centers for the second layer and, as the surface composition confirms the formation of the TiO₂ film, these can support the development of good interfaces between the two layers. The surface composition shows no carbon traces left from the organic precursor system but a rather high percentage of Sn from the FTO substrate that suggests the development of a very thin first layer (Table 1 SEM cross-section, right image). Moreover, the FTO layer is very thin as the silicon (Si) element from the glass substrate could be sensed. The low roughness (RMS) value confirms the morphology with very small surface aggregates.

The SEM images of the composite with GO filler in Figure 4b–e outlines the characteristic dendritic shape of the GO plates (according to the GO filler image in Figure 4g left) loaded with TiO₂. The layers are uniform and compact with less randomly distributed surface aggregates for the composites with 5%_w and 10%_w GO, as result of a higher likelihood of forming C–O–Ti bonds because of the higher filler content; this confirms that good interfaces are well developed in the composite(s) with a higher filler content as the TiO₂ aggregates no longer tend to form large agglomerates as in the case of the composites with 1.4%_w and 3%_w GO. The SEM images also outline similarities among the sample without filler and the composite with 1.4%_w GO. It is thus expected that the composite with a higher GO content will better perform in the photocatalytic processes and will be more stable in the aqueous medium, in continuous flow operation.





(h) Cross-section for the composite thin film FTO/TiO₂/TiO₂-GO 5%_{ow}

Figure 4. SEM images of the thin films before and after the three photocatalytic cycles (a–f), detailed images of the fillers (g) and a cross section of the FTO/TiO₂/TiO₂-GO 5%_{ow} thin film (h).

The cross-section image of the composite thin film with 5%_{ow} GO shows a good compatibility between the two layers as not any discontinuities (gaps) could be noticed.

The images of the composite with rGO filler in Figure 4f show the deposition of many TiO₂ agglomerates on the rGO sheets (according to the rGO surface in Figure 4g right). The rGO sheets are fully covered with the large aggregates of TiO₂ suggesting that good interfaces are developed between the matrix and the filler sheets.

As outlined by the SEM images in Figure 4b–e, the composites with GO filler have a good stability as the results are quite similar comparing the images of the films before and after the photocatalytic cycles. The composite with 1.4%_{ow} GO seems to be mostly affected as the images in Figure 4b outline the development of cracks (yellow arrows) during the cycles. The TiO₂-rGO composite also outlines, in Figure 4f, fine cracks after the second and the third photocatalytic cycles, suggesting the lower stability of this thin film during the process.

The surface composition results (Table 2) show a low content of Carbon (C) in the bi-layered thin film without GO or rGO filler due to the traces from the sol precursors system that were not completely decomposed/removed at the thermal treatment temperature (150 °C). The content of Carbon could be mainly noticed near the surface aggregates where

a larger amount of precursor system could collect and could be further only partially decomposed. Supporting this idea, the rather high carbon content in the composite with 1.4%_w GO may be the result of the surface agglomerates on the thin film. The content of C in the absence of the surface aggregates on the composites with 5%_w and 10%_w GO content confirms the development of the composites with the filler loaded with TiO₂ and of some carbon traces left from the sol. The higher Ti content in the composites with 1.4%_w and 3%_w GO compared with the 5%_w and 10%_w ones confirms that the aggregates are only containing TiO₂. The Ti content in the TiO₂-rGO composite is higher than in the composite containing 5%_w GO, confirming the compact deposition of the matrix on the rGO sheets. This is also outlined when comparing the carbon content in the composite with 5%_w GO vs. 5%_w rGO when the rGO chemical structure should provide a higher C content but the EDX results show a lower carbon percentage value as result of the denser structure in the composite matrix.

The surface composition initially recorded on the films did not outline any Sulphur (S) content. After photocatalysis, the results in Table 2 show a very low S percentage that can be the result of the adsorbed by-products left at the surface after methylene blue decomposition and/or of the unreacted pollutant adsorbed at the thin film's surface; moreover, this very low content outlines that the pollutant was well decomposed under irradiation, towards mineralization.

Table 2. Elemental surface composition, roughness and PZC of the films before and after each photocatalytic cycle.

Thin Film	Process Parameter	Elemental Average Surface Composition [at%]					RMS [nm]	PZC
		C	Ti	O	F, Sn, Si	S		
FTO/TiO ₂ /TiO ₂ no filler	Before photocatalysis	3.14	31.12	61.79	3.95	-	192.1	6.63
	After Cycle 1	1.61	30.23	62.09	5.96	0.12	215.8	
	After Cycle 2	1.53	30.07	63.03	4.96	0.41	227.5	
	After Cycle 3	1.03	28.79	63.00	7.19	0.00	205.1	
FTO/TiO ₂ /TiO ₂ -GO 1.4% _w	Before photocatalysis	8.44	30.86	57.38	3.33	-	230.3	7.25
	After Cycle 1	5.07	31.75	60.51	2.67	0.00	364.4	
	After Cycle 2	5.12	26.87	63.71	4.28	0.02	304.1	
	After Cycle 3	5.08	27.57	62.51	4.83	0.01	297.1	
FTO/TiO ₂ /TiO ₂ -GO 3% _w	Before photocatalysis	3.63	34.09	56.72	5.56	-	128.4	7.58
	After Cycle 1	4.65	28.44	60.74	6.09	0.09	197.8	
	After Cycle 2	3.14	27.16	63.23	6.33	0.14	204.4	
	After Cycle 3	2.35	26.68	62.18	8.60	0.20	169.7	
FTO/TiO ₂ /TiO ₂ -GO 5% _w	Before photocatalysis	7.58	26.81	59.69	5.92	-	125.5	8.01
	After Cycle 1	5.00	28.04	63.28	3.57	0.12	163.8	
	After Cycle 2	4.01	27.35	63.31	5.20	0.13	153.5	
	After Cycle 3	4.13	28.82	63.06	3.82	0.16	148.9	
FTO/TiO ₂ /TiO ₂ -GO 10% _w	Before photocatalysis	8.79	27.39	59.96	3.87	-	139.8	8.33
	After Cycle 1	6.11	27.70	61.27	4.74	0.17	190.2	
	After Cycle 2	4.56	27.96	62.73	4.70	0.05	184.9	
	After Cycle 3	4.82	27.91	62.64	4.52	0.11	156.1	
FTO/TiO ₂ /TiO ₂ -rGO 5% _w	Before photocatalysis	5.48	32.76	58.37	3.38	-	146.6	7.37
	After Cycle 1	6.16	29.70	59.75	4.21	0.18	128.3	
	After Cycle 2	4.63	27.62	62.68	4.89	0.18	120.3	
	After Cycle 3	3.23	26.41	63.52	6.80	0.03	113.4	

In Table 2 are also recorded the average roughness values (RMS) of the thin films. The results outline a rather rough surface of the photocatalysts that can support the adsorption of the pollutants very well. These RMS values outline major differences between the thin films with various filler content, mainly because of the larger agglomerations shown in the SEM images for the composite with 1.4%_w GO (Figure 4b). However, while it can be expected that using this rougher composite film, the

photocatalysis efficiency will be higher supporting the adsorption in the first step of the process, the stability of this film may be lower.

The EDX results recorded after the photocatalytic cycles outline a decrease in the Ti content, mainly for the composites with 1.4%_w and 3%_w GO, suggesting that some of the TiO₂ agglomerations may be detached from the graphene derivative's surface, to most likely end up in the solution of the pollutant, thus the stability of these materials can be subject to improvement.

The slight decrease in the C content of the thin films after the photocatalytic cycles (Table 2) may be the result of the diffusion of the organic slightly soluble compounds from the sol precursors into the MB solution; this assumption is confirmed also by the similar trend observed on the sample without (r)GO filler.

The titanium content in the TiO₂-rGO composite follows a constant slight decrease after each photocatalytic cycle suggesting that fine titania particles are leaving the rGO surface into the MB solution as also outlined by the RMS decrease (Table 2), supporting the conclusion of a lower stability of this composite film.

The increase in the roughness (RMS) values after the first two photocatalytic cycles for the TiO₂-GO composites supports the idea of a partial dislocation of the aggregates mainly from the FTO/TiO₂/TiO₂-GO 1.4%_w and from the FTO/TiO₂/TiO₂-GO 3%_w composites surface. The lowest roughness variation among the photocatalytic cycles was recorded for the FTO/TiO₂/TiO₂-GO 5%_w composite, confirming its good stability.

The photoactivity of the films was checked following their efficiency when using the standard methylene blue pollutant solution (MB, 10 ppm) at an optimized pH value of the pollutant solution. The composite thin films had PZC values ranging between 7.25...8.33 (Table 2). At pH values higher than these, the composites surface is "negatively charged" and the MB molecules are "positively charged" thus supporting the electrostatic interactions. Hence, the optimum pH of the pollutant solution was selected to be 8.50.

The water contact angle (WCA) variation results (Table 3) outline that, before photocatalysis, the highest value was recorded for the thin films with rGO filler because of the lower polarity of this filler. This composite seems to follow the Cassie-Baxter mechanism [29], as, despite the higher RMS value, it acts as a less hydrophilic surface compared to the composites with 3%_w, 5%_w and 10%_w GO content.

Table 3. Water contact angle (WCA) of the thin films exposed to UV and UV + VIS radiation.

Thin Film	WCA θ [°]					
	Before Photo-Catalysis	After 1h of UV Conditioning	After Cycle 1 + 2h of UV + VIS Conditioning and Regeneration		After Cycle 2 + 2h of UV + VIS Conditioning and Regeneration	
			After Cycle 1	After Cycle 2	After Cycle 1	After Cycle 2
(a) FTO/TiO ₂ /TiO ₂ no filler	14.4	2.8	10.4	3.5	10.2	3.5
(b) FTO/TiO ₂ /TiO ₂ -GO 1.4% _w	12.2	<1	10.6	<1	32.1	<4
(c) FTO/TiO ₂ /TiO ₂ -GO 3% _w	7.1	<1	8.3	<1	9.1	<1
(d) FTO/TiO ₂ /TiO ₂ -GO 5% _w	8.1	<1	9.8	2.4	10.9	<1
(e) FTO/TiO ₂ /TiO ₂ -GO 10% _w	6.9	<1	6.7	1	7.3	<1
(f) FTO/TiO ₂ /TiO ₂ -rGO 5% _w	19.6	6.2	10.2	3.7	7.3	3.9

The experiments with the conditioned thin films show that super-hydrophilicity is induced after one hour of UV irradiation ($G_{UV} = 23 \text{ W/m}^2$) before the first photocatalytic cycle. Before the second and the third cycle the conditioning treatment was done using UV + VIS radiation for 2 h ($G_{UV + VIS} = 810 \text{ W/m}^2$) to induce a strong hydrophilicity along with the elimination of possible residual products left on the surface of the photocatalyst. The results show that super-hydrophilicity ($\text{WCA} < 10^\circ$) was reached each time, although after the second cycle the sample with 1.4%_w GO content shows a significant increase in the WCA value as a consequence of the adsorbed by-products at the surface.

When using high or low filler amounts, the composites perform better than the pure TiO_2 outlined by the difference in the photocatalytic efficiency when using TiO_2 compared with the composite thin films (two times higher efficiencies for the composite with 10%_w GO under simulated solar radiation conditions compared with the pure TiO_2).

The results in Figure 5, Cycle 1 outline that the photocatalytic efficiency increases with the GO content in the composite. The sample with 10%_w GO supports the highest adsorption efficiency. A higher filler content may have as consequence a higher likelihood to develop more Ti-O-C bonds and thus to increase the number of spots where the electrostatic attraction between the negatively charged photocatalytic surface and the positively charged MB pollutant may occur. However, the adsorption results show the highest efficiency in the second and third cycle for the $\text{FTO/TiO}_2/\text{TiO}_2\text{-GO}$ 1.4%_w composite, although the overall efficiency after 5 h of irradiation proves that adsorption is not the governing factor influencing the photocatalytic efficiency.

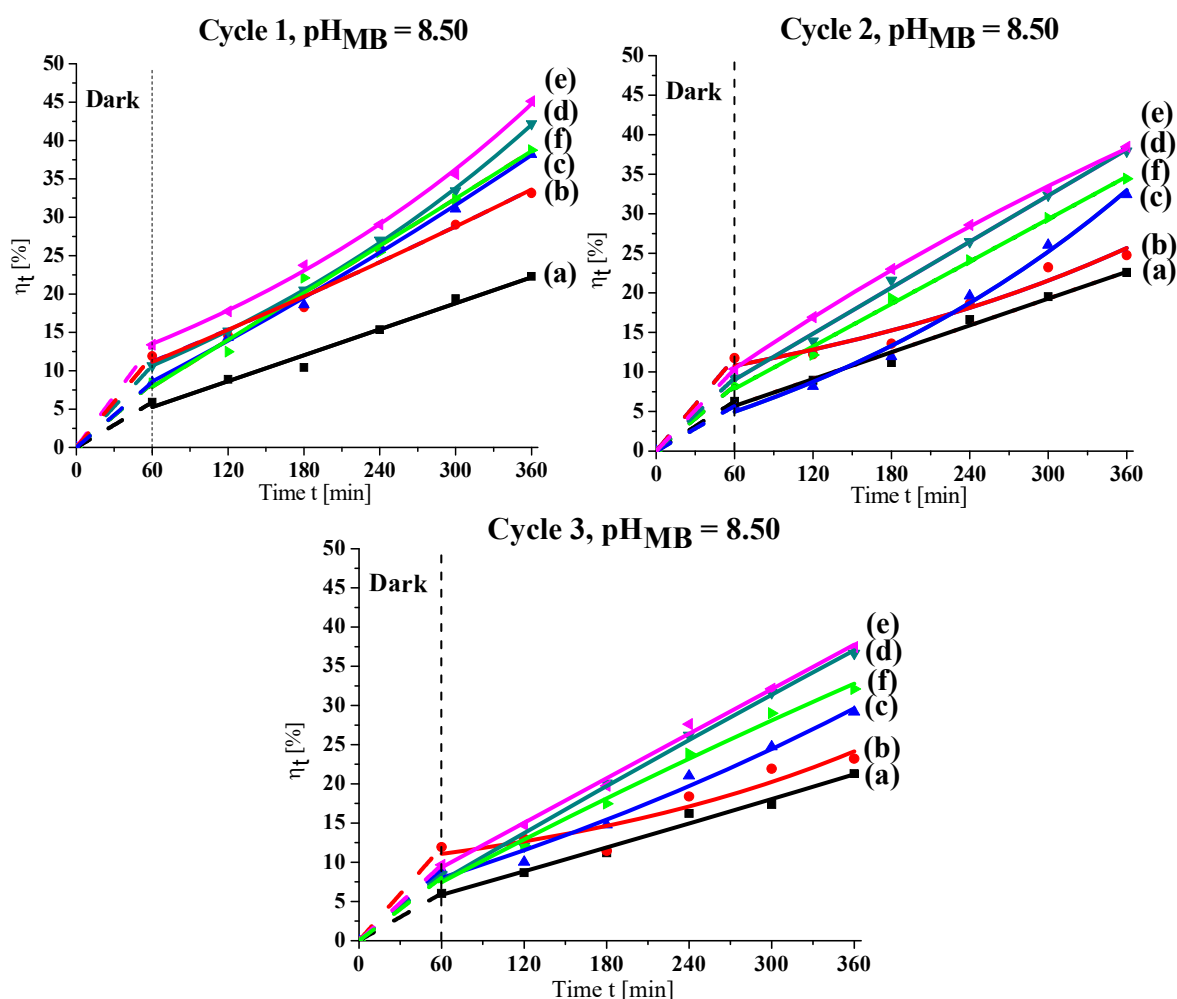


Figure 5. Efficiencies of the MB removal for three successive photocatalytic cycles in dynamic regime on: (a) $\text{FTO/TiO}_2/\text{TiO}_2$ no filler; (b) $\text{FTO/TiO}_2/\text{TiO}_2\text{-GO}$ 1.4%_w; (c) $\text{FTO/TiO}_2/\text{TiO}_2\text{-GO}$ 3%_w; (d) $\text{FTO/TiO}_2/\text{TiO}_2\text{-GO}$ 5%_w; (e) $\text{FTO/TiO}_2/\text{TiO}_2\text{-GO}$ 10%_w; (f) $\text{FTO/TiO}_2/\text{TiO}_2\text{-rGO}$ 5%_w.

The photocatalysis results also confirm the crystallinity degree role in the efficiency of the process. As the results recorded in Figure 3I outline, the thin films with 5%_w and 10%_w GO had the higher percentage of crystallinity thus these composites may well support the mobility of the electron-hole pairs and better limit their recombination. This effect led to the obtaining of the highest process efficiencies when using these two composites.

By comparing the results recorded during the second photocatalytic cycle with those observed during the first cycle, it can be noted that, for the catalyst with a lower GO content in Figure 5–Cycle 2, graphs (b) and (c), the thin film activation took longer possibly because part of the adsorption sites were clogged with residual products that had to be firstly degraded, suggesting that in these cases, the irradiated substrate requires a longer regeneration duration for reaching the optimal removal conditions. The FTO/TiO₂/TiO₂-GO 1.4%_w thin film did not support good results as the efficiency significantly decreased, being close to that of the sample without filler. A small efficiency decrease during the second cycle was also noticed when using the composites with 3%_w...10%_w GO, and also the composite with 5%_w rGO. The samples with 5%_w and 10%_w GO turned out to be the best options for the photocatalytic process in dynamic regime, as in the third cycle they behave almost identically, supporting the best MB removal efficiencies. The results observed when using a different filler with the same filler content (5%_w GO vs. 5%_w rGO) outline lower efficiencies for the rGO filler, as the results in graph (f) Figure 5 show, which can be correlated with the lower rGO polarity but also with a slightly lower crystallinity degree.

The reaction rate constants (*k*) for the MB removal using different photocatalysts and the correlation coefficient (*R*²) values are included in Table 4. The *R*² values close to 1 demonstrate that the dye degradation follows the pseudo first order kinetic. Considering the values of the reaction rate constants along with the 95% confidence interval, it may be concluded that the best reaction conditions were met when using the samples with 10%_w and 5%_w GO in the composite layer.

Table 4. Reaction rate constant (*k*) (±95% confidence interval) and correlation coefficient (*R*²) for the MB degradation using the thin films.

Thin Film	<i>R</i> ²	<i>k</i> ·10 ^{−4}
(a) FTO/TiO ₂ /TiO ₂ no filler	0.97802	6.200 ± 0.007
(b) FTO/TiO ₂ /TiO ₂ -GO 1.4% _w	0.98409	9.430 ± 0.009
(c) FTO/TiO ₂ /TiO ₂ -GO 3% _w	0.97460	11.800 ± 0.007
(d) FTO/TiO ₂ /TiO ₂ -GO 5% _w	0.96174	13.000 ± 0.015
(e) FTO/TiO ₂ /TiO ₂ -GO 10% _w	0.96064	13.600 ± 0.020
(f) FTO/TiO ₂ /TiO ₂ -rGO 5% _w	0.97697	12.400 ± 0.015

The absorbance spectra in Figure 6 for the FTO/TiO₂/TiO₂-GO10%_w thin film after photocatalysis and after regeneration using UV + VIS radiation were recorded after the first and after the second photocatalytic cycles. After photocatalysis, the surface shows light blue traces of unreacted MB while the results after UV + VIS irradiation indicate a regeneration/self-cleaning efficiency higher than 90%, suggesting that regeneration is required after each photocatalytic cycle, for 2 h under UV + VIS irradiation, when using high irradiance values.

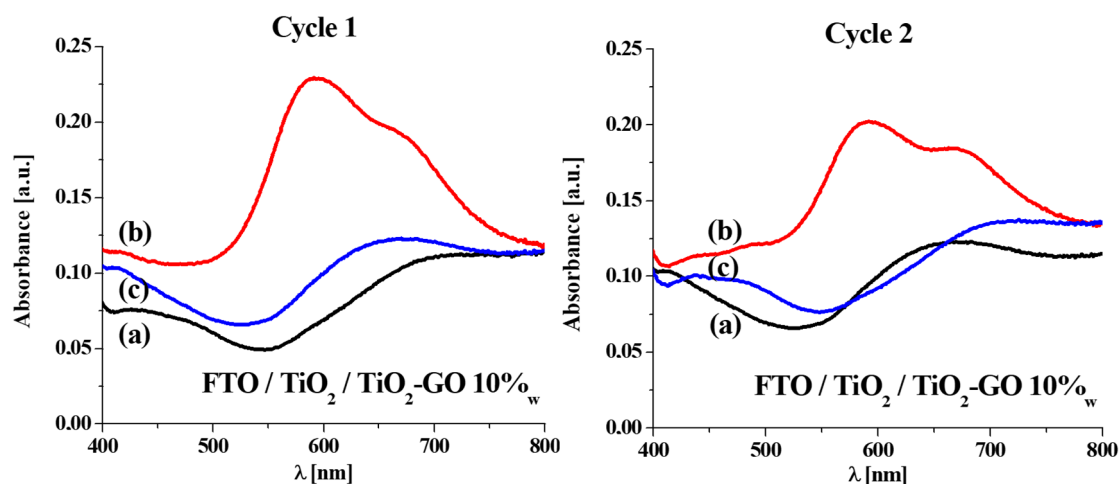


Figure 6. Absorbance spectra recorded on the FTO/TiO₂/TiO₂-GO 10%_w composite for Cycle 1 and Cycle 2 (a) before photocatalysis; (b) after photocatalysis and (c) after photocatalysis + regeneration.

The results recorded in the static regime (Table 5) indicate the Vis-activation of the GO composites through the development of the diode-type junction(s), as higher efficiencies in MB removal were recorded under UV + VIS radiation (at low irradiance value) compared to UV. The possible dye sensitization was previously investigated by comparing the results with those recorded when using a colorless pollutant (imidacloprid). The results outlined that a dye sensitization may occur as these systems proved to be Vis-active [19]. Vis-activation was weaker for the rGO containing composite, suggesting the lower compatibility of the TiO₂ matrix with the less polar rGO filler. As the data in Table 5 show, almost similar values were recorded when using the sample without filler both under UV and under UV + VIS irradiation, outlining that the factor majorly responsible for the TiO₂ activation is the UV irradiation.

Table 5. Efficiencies of the MB removal in static regime.

Thin Film	Type of Irradiation	Photocatalytic Efficiency [%]					
		1h Dark	1h Irradiation	2h Irradiation	3h Irradiation	4h Irradiation	5h Irradiation
(a) FTO/TiO ₂ /TiO ₂ no filler LAB	UV + VIS	6,78	7,97	9,01	14,20	16,03	17,66
	UV	6,71	7,24	9,79	15,98	16,72	16,89
(b) FTO/TiO ₂ /TiO ₂ -GO 1.4% _w LAB	UV + VIS	8,98	11,50	16,50	20,18	22,77	24,83
	UV	8,33	10,25	12,43	15,44	17,70	20,99
(c) FTO/TiO ₂ /TiO ₂ -GO 3% _w LAB	UV + VIS	14,19	18,53	22,69	24,72	28,29	30,73
	UV	14,74	15,17	17,95	19,81	20,20	21,67
(d) FTO/TiO ₂ /TiO ₂ -GO 5% _w LAB	UV + VIS	13,08	17,30	22,11	25,65	30,54	31,76
	UV	12,41	13,93	15,47	16,60	19,49	22,28
(e) FTO/TiO ₂ /TiO ₂ -GO 10% _w LAB	UV + VIS	13,78	17,23	21,68	25,04	28,49	31,33
	UV	13,79	15,81	18,36	19,35	21,48	24,19
(f) FTO/TiO ₂ /TiO ₂ -rGO 5% _w LAB	UV + VIS	12,17	14,78	17,78	20,74	23,20	25,54
	UV	12,12	15,71	17,84	20,26	22,10	23,39

The photocatalytic results in dynamic (Figure 5) and in static regime (Table 5) outline an efficiency increase of about ~15% recorded for the samples with 10%_w GO and with 5%_w GO. Considering the similar value of the ratio between the volume of the pollutant and the area of the film for the two cases (static and dynamic regime), the much higher irradiance value in the dynamic process is expected to lead to much higher process efficiencies. However, the rather small efficiency increase may be the result of the fast recombination of the charge carriers that can recombine before taking part in the chemical

reactions through which the oxidation species are formed but also because of the continuous flow condition.

4. Conclusions

Two-layered $\text{TiO}_2/\text{TiO}_2\text{-GO}$ and $\text{TiO}_2/\text{TiO}_2\text{-rGO}$ composites were obtained using SPD and coupled with sol spraying synthesis. All the composites were VIS-active in static regime through the development of a diode-type structure. The results proved that the VIS-activation is sensitive to the filler polarity as the composites with GO filler led to higher photocatalytic efficiencies compared to those using the rGO filler, under UV + VIS irradiation.

The photocatalytic efficiencies recorded in continuous flow operation (dynamic regime) showed significantly higher MB removal efficiencies when increasing the GO content in the composite layer(s). The samples with 5%_w and 10%_w GO proved the highest removal efficiency during the first photocatalytic cycle following the increased crystallinity that may support the flow of the electron-hole pairs, reducing their recombination, along with the higher polarity of this filler that supports the increased compatibility between the matrix and the filler, and thus, the composite stability. For the composite with rGO filler, the efficiencies in MB removal are almost similar under UV + Vis and under UV irradiation in static and in dynamic regimes suggesting the lower compatibility between the ionic TiO_2 matrix and the rather non-polar rGO filler.

The efficiencies in the dynamic regime compared to those recorded in the static regime outline an increase of only ~15% although the irradiance value was about 15 times higher during the dynamic regime experiments, possibly due to a significant recombination of the charge carriers and also due to the continuous flow conditions.

During the second and the third photocatalytic cycles the $\text{FTO}/\text{TiO}_2/\text{TiO}_2\text{-GO}$ 5%_w and the $\text{FTO}/\text{TiO}_2/\text{TiO}_2\text{-GO}$ 10%_w composite layers proved similar efficiencies, allowing us to recommend the composite with 5%_w GO content to be used in the advanced wastewater treatment because of its efficiency, good stability and lower cost.

The good stability of the composite in the aqueous environment was confirmed by the SEM images recorded before and after each of the three photocatalytic cycles. The surface composition shows a slight decrease in the titanium and carbon content due to a possible partial wash out of the titania surface aggregates and of the organic compounds remaining from the sol precursor. This phenomenon mainly occurs on the composite films with low GO content and the one with rGO filler, supporting the recommendation of the $\text{FTO}/\text{TiO}_2/\text{TiO}_2\text{-GO}$ 5%_w composite for up scaled applications.

Author Contributions: Conceptualization, A.D.; Methodology, A.D.; Validation, A.C.O. and O.B.; Investigation, I.T.; Writing—original draft, I.T.; Writing—review & editing, A.D.; Supervision, A.D. All authors have read and agreed to the published version of the manuscript.

Funding: This work was supported by the grant of the Romanian Ministry of Research and Innovation, CCCDI-UEFISCDI, project number PN-III-P1- 1.2-PCCDI-2017-0619, contract no. 42 PCCDI/2018 within PNCDI that is gratefully acknowledged

Institutional Review Board Statement: Not applicable

Informed Consent Statement: Not applicable

Data Availability Statement: Not applicable

Acknowledgments: This work was supported by the grant of the Romanian Ministry of Research and Innovation, CCCDI-UEFISCDI, project number PN-III-P1-1.2-PCCDI-2017-0619, contract no. 42 PCCDI/2018 within PNCDI that is gratefully acknowledged.

Conflicts of Interest: The authors declare no conflict of interest

References

- Dwevedi, A.; Kayastha, A.M. Wastewater remediation via combo-technology. In *Solutions to Environmental Problems Involving Nanotechnology and Enzyme Technology*; Dwevedi, A., Ed.; Academic Press: Cambridge, MA, USA, 2019; pp. 91–126.
- Saravanan, A.; Kumar, P.S.; Vo, D.V.N.; Yaashikaa, P.R.; Karishma, S.; Jeevanantham, S.; Gayathri, B.; Bharathi, V.D. Photocatalysis for removal of environmental pollutants and fuel production: A review. *Environ. Chem. Lett.* **2020**, *19*, 441–463. <https://doi.org/10.1007/s10311-020-01077-8>.
- Koe, W.S.; Lee, J.W.; Chong, W.C.; Pang, Y.L.; Sim, L.C. An overview of photocatalytic degradation: Photocatalysts, mechanisms, and development of photocatalytic membrane. *Environ. Sci. Poll. Res.* **2020**, *27*, 2522–2565.
- Du, Y.B.; Zhang, L.; Ruan, M.; Niu, C.G.; Wen, X.J.; Liang, C.; Zhang, X.G.; Zeng, G.M. Template-free synthesis of three-dimensional porous CdS/TiO₂ with high stability and excellent visible photocatalytic activity. *Mater. Chem. Phys.* **2018**, *212*, 69–77.
- Shehzad, N.; Tahir, M.; Johari, K.; Murugesan, T.; Hussain, M. A critical review on TiO₂ based photocatalytic CO₂ reduction system: Strategies to improve efficiency. *J. CO₂ Util.* **2018**, *26*, 98–122.
- Bisaria, K.; Sinha, S.; Singh, R.; Iqbal, H.M.N. Recent advances in structural modifications of photo-catalysts for organic pollutants degradation—A comprehensive review. *Chemosphere* **2021**, *284*, 131263.
- Junaidi, N.F.D.; Othman, N.H.; Fuzil, N.S.; Shayuti, M.S.M.; Alias, N.H.; Shahrudin, M.Z.; Marpani, F.; Lau, W.J.; Ismail, A.F.; Aba, N.F.D. Recent development of graphene oxide-based membranes for oil–water separation: A review. *Sep. Purif. Technol.* **2021**, *258*, 118000.
- Xu, Q.; Zhang, L.; Yu, J.; Wageh, S.; Al-Ghamdi, A.A.; Jaroniec, M. Direct Z-scheme photocatalysts: Principles, synthesis, and applications. *Mater. Today* **2018**, *21*, 1042–1063.
- Qi, K.; Cheng, B.; Yu, J.; Ho, W. A review on TiO₂-based Z-scheme photocatalysts. *Chinese J. Catal.* **2017**, *38*, 1936–1955.
- Ibrahim, Y.O.; Hezam, A.; Qahtan, T.F.; Al-Aswad, A.H.; Gondal, M.A.; Drmosh, Q.A. Laser-Assisted Synthesis of Z-Scheme TiO₂/rGO/gC₃N₄ Nanocomposites for Highly Enhanced Photocatalytic Hydrogen Evolution. *Appl. Surf. Sci.* **2020**, *534*, 147578. <https://doi.org/10.1016/j.apsusc.2020.147578>.
- Mohammadi, M.; Roknabadi, M.R.; Behdani, M.; Kompany, A. Enhancement of visible and UV light photocatalytic activity of rGO-TiO₂ nanocomposites: The effect of TiO₂/Graphene oxide weight ratio. *Ceram. Int.* **2019**, *45*, 12625–12634.
- Ramos, D.K.C.; González, M.V.; Muñoz, R.A.E.; Cruz, J.S.; De Moure-Flores, F.J.; Mayén-Hernández, S.A. Obtaining and Characterization of TiO₂-GO Composites for Photocatalytic Applications. *Int. J. Photoenergy* **2020**, *2020*, 3489218. <https://doi.org/10.1155/2020/3489218>.
- Ye, X.; Chen, L.; Wang, Z.; Wang, Q.; Xiao, X.; Liu, X. Facile in situ hydrothermal synthesis of titania nanosheets on reduced graphene oxide with photocatalytic activity. *J. Photochem. Photobiol. A: Chem.* **2019**, *385*, 112085. <https://doi.org/10.1016/j.jphotochem.2019.112085>.
- Lesiak, B.; Kövér, L.; Tóth, J.; Zemek, J.; Jiricek, P.; Kromka, A.; Rangan, N. C sp²/sp³ hybridisations in carbon nanomaterials—XPS and (X)AES study. *Appl. Surf. Sci.* **2018**, *452*, 223–231.
- Boukhvalov, D.W.; Katsnelson, M.I. Modeling of Graphite Oxide. *J. Am. Chem. Soc.* **2008**, *130*, 10697–10701.
- Andronic, L.; Isac, L.; Miralles-Cuevas, S.; Visa, M.; Oller, I.; Duta, A.; Malato, S. Pilot-plant evaluation of TiO₂ and TiO₂-based hybrid photocatalysts for solar treatment of polluted water. *J. Hazard. Mater.* **2016**, *320*, 469–478.
- Plantard, G.; Dezani, C.; Ribeiro, E.; Reoyo-Prats, B.; Goetz, V. Modelling heterogeneous photocatalytic oxidation using suspended TiO₂ in a photoreactor working in continuous mode: Application to dynamic irradiation conditions simulating typical days in July and February. *Can. J. Chem. Eng.* **2021**, *99*, 142–152.
- Sengupta, I.; Chakraborty, S.; Talukdar, M. Thermal reduction of graphene oxide: How temperature influences purity. *J. Mater. Res.* **2018**, *33*, 4113–4122.
- Tismanar, I.; Obreja, A.C.; Buiu, O.; Duta, A. VIS-active TiO₂–graphene oxide composite thin films for photocatalytic applications. *Appl. Surf. Sci.* **2021**, *538*, 147833. <https://doi.org/10.1016/j.apsusc.2020.147833>.
- International Standard ISO 10678:2010; Fine Ceramics (Advanced Ceramics, Advanced Technical Ceramics)—Determination of Photocatalytic Activity of Surfaces in an Aqueous Medium by Degradation of Methylene Blue.
- Bogatu, C.; Covei, M.; Tismanar, I.; Perniu, D.; Duta, A. Composite nanostructures as potential materials for water and air cleaning with enhanced efficiency. In *Advanced Nanostructures for Environmental Health*; Baia, L., Pap, Z., Hernadi, K., Baia, M., Eds.; Elsevier: Amsterdam, The Netherlands, 2020; pp. 431–464.
- Hummers, W.S.; Offeman, R.E. Preparation of Graphitic Oxide. *J. Am. Chem. Soc.* **1958**, *80*, 1339–1339.
- Bragaru, A.; Vasile, E.; Obreja, C.; Kusko, M.; Danila, M.; Radoi, A. Pt nanoparticles on graphene—Polyelectrolyte nanocomposite: Investigation of H₂O₂ and methanol electrocatalysis. *Mater. Chem. Phys.* **2014**, *146*, 538–544.
- Prabhu, S.; Cindrella, L.; Kwon, O.J.; Mohanraju, K. Superhydrophilic and self-cleaning rGO-TiO₂ composite coatings for indoor and outdoor photovoltaic applications. *Sol. Energy Mater. Sol. Cells* **2017**, *169*, 304–312.
- Alkaykh, S.; Mbarek, A.; Ali-Shattle, E.E. Photocatalytic degradation of methylene blue dye in aqueous solution by MnTiO₃ nanoparticles under sunlight irradiation. *Heliyon* **2020**, *6*, e03663. <https://doi.org/10.1016/j.heliyon.2020.e03663>.
- Raheb, I.; Manlla, M.S. Kinetic and thermodynamic studies of the degradation of methylene blue by photo-Fenton reaction. *Heliyon* **2021**, *7*, e07427. <https://doi.org/10.1016/j.heliyon.2021.e07427>.

27. Tabarsa, M.; ZareNezhad, B. An eco-friendly air–water plasma surface treatment technique for improving the stability of graphene oxide nanosheets in aqueous solutions. *Mater. Today Commun.* **2020**, *26*, 101940. <https://doi.org/10.1016/j.mtcomm.2020.101940>.
28. Wei, L.; Chen, S.; Yang, Y.; Dong, Y.; Song, W.; Fan, R.. Reduced graphene oxide modified TiO₂ semiconductor materials for dye-sensitized solar cells. *RSC Adv.* **2016**, *6*, 100866–100875.
29. Banerjee, S.; Dionysiou, D.D.; Pillai, S.C. Self-cleaning applications of TiO₂ by photo-induced hydrophilicity and photocatalysis. *Appl. Catal. B Environ.* **2015**, *176–177*, 396–428.